Hindawi
Advances in Condensed Matter Physics
Volume 2023, Article ID 3179210, 12 pages
https://doi.org/10.1155/2023/3179210

*Research Article*

# Structural, Electronic, Dynamic, and Optical Properties of 2D Monolayer Tungsten Telluride (2H-$WTe_2$) under Small Biaxial Strain Using Density Functional Theory (DFT and DFT + U)

**Mulugeta Woldesenbet, Nebiyu Debelo, and Menberu Woldemariam**

*Department of Physics, Jimma University, P.O. Box 378, Jimma, Ethiopia*

Correspondence should be addressed to Menberu Woldemariam; menberu.mengesha@ju.edu.et

Received 8 September 2023; Revised 10 October 2023; Accepted 31 October 2023; Published 23 November 2023

Academic Editor: Tholkappiyan Ramachandran



The structural, electronic, vibrational, and optical properties of 2D- 2H-$WTe_2$ monolayer are investigated using density functional theory with respect to a plane wave ultrasoft pseudopotentials (PW-USPPs) in a generalized gradient approximation (GGA) and with the Hubbard potential (GGA + U). The equilibrium state properties such as lattice parameters, unit cell volume, bulk modulus, and its derivative are determined. The band gap values of monolayer 2H-$WTe_2$ are investigated for unstrained, 2% biaxial compression, and biaxial tensile stress using GGA, respectively. The obtained band gap values of 2H-$WTe_2$ with respect to GGA are 1.043, 1.1487, and 0.9439 eV for unstrained, biaxial compression, and tensile strain, respectively. Moreover, the band gap values determined using Hubbard correction (GGA + U) are 1.1089 eV (unstrained), 1.2332 eV (2% biaxial compression), and 0.9945 eV (2% biaxial tensile stress), respectively. The band gap value obtained using Hubbard correction predicts the experimental value more precisely. The projected density of state shows W (3d) orbital is more dominant both in the valence band maximum and conduction band minimum. Moreover, a small amount of tensile or compressive strain is used to tune the band gap of the monolayer without affecting its direct band gap nature. In addition to this, the phonon dispersion and optical properties are discussed for tensile strain, unstrained, and compressive strain, respectively.

## 1. Introduction

Due to their tunable direct band gaps, monolayer transition metal dichalcogenides (TMDs) are a preferred family of two-dimensional (2D) materials. The range of band gap values of 2D transition metal dichalcogenides made them an interesting material for technological applications in optoelectronic and photovoltaic devices [1, 2]. Due to their significant chemical and physical features molybdenum and tungsten dichalcogenides ($MoS_2$, $MoSe_2$, $WS_2$, and $WSe_2$) with a band gap of 1.88, 1.57, 2.03, and 1.67, respectively, have received high attention as a 2D layered material [3]. These band gap values fall within the band gap value of ideal photovoltaic materials (1–1.8 eV) [4]. Moreover, 2D layered structures enable doping with the additional atoms in substitution of one or more atoms to adjust and tune its electronic and optical properties [5, 6]

The hexagonal tungsten ditelluride is one among the family of materials composed of $WX_2$ (W-tungsten and chalcogens $X = S, Se, Te$), which have been made from a 2D slab of layers with strong covalent bonds which are stacked together with the weak van-der Waals force with the next layer. The 2D-$WTe_2$ has the highest mobility among this family because of its lowest effective mass [7]. On the other hand, strain is vigorous in enhancing device performance because it alters the band structure, electron mobility, and other important properties of 2D-TMDs in general and it is also essential in the case of 2D-$WTe_2$ [8, 9]. One of the most obvious ways to acquire a broad range of tunability in electronic and optical properties is to manipulate the band gap of two-dimensional materials by strain in addition to doping and other techniques. Strain engineering is one of the powerful methods for tuning the band gap and significant performance enhancement of electronic and optoelectronic devices [10].

DFT simulations were used to determine the optical absorption characteristics of $WS_2$, and these characteristics make $WS_2$ a promising photovoltaic material [11]. $MoS_2$, $MoSe_2$, $WS_2$, and $WSe_2$ monolayers complex dielectric functions for photon energies between 1.5 and 3.0 eV have been experimentally calculated. These four materials have a peak absorbance of more than 15% and the dielectric functions predict extensive light-matter interactions in the monolayers. Exciton splitting is extrapolated from the measured dielectric function in conformity with density functional models [12]. For 2D-$MoSe_2$ and 2D-$WSe_2$, the biaxial strain has been used to identify the direct-to-indirect band gap transition in the compressive strain. It has also been reported that the peaks for real and imaginary values of the dielectric constant, optical absorption, and electron energy loss spectra, may allow for appealing applications for photovoltaic and electroluminescent devices. They were strong prospects for digital electronics and optoelectronics device applications due to their optical performance and light absorption under tensile strain [13]. However, most of the studies on $WTe_2$ did not consider the consequences of the residual self-interaction. One of the corrective schemes widely used to alleviate the challenges of residual self-interaction is the GGA + U approach [14, 15]. Moreover, the density functional perturbation theory (DFPT) with Hubbard correction (DFPT + U functional) [16] gives more precise results for phonon dispersion as compared to the DFPT [17].

In this study, we have investigated the structural, electronic, vibrational, and optical properties of 2H-$WTe_2$ (space group p63/mmc) for photovoltaic applications and digital electronics using density functional theory (DFT) and time-dependent density functional theory (TD-DFT) with the help of a plane wave ultrasoft pseudopotentials (PW-USPPs). The structural, electronic, vibrational, and optical properties are investigated in detail. The structural and electronic properties are investigated using the approximations GGA [18] and GGA + U [14, 15] for exchange-correlation potential. Moreover, the effect of tensile or compressive strain on the electronic structure of $WTe_2$ is determined. The phonon dispersion is calculated using DFPT and DFPT + U. The optical properties are determined using TD-DFPT. Finally, the obtained results are compared with the existing experimental and theoretical results.

## 2. Computational Details

In this study we have used DFT with the implementation of Quantum Espresso (QE) package [19, 20], applying the generalized gradient approximation (GGA) with the Perdew–Burke–Ernzerhof (PBE) functional and including the Hubbard correction GGA + U for the electron exchange-correlation interactions. Here we have used GGA + U since our material contains a transition heavy metal W which has high-electron–electron correlations. The pseudopotential developed for the QE package (PBE QE UPF) from the standard solid-state pseudopotential (SSSP) library is used [21]. The corresponding valence electrons considered for the calculations are W-[Xe] $4f^{14}$ $5d^4$ $6s^2$, and Te-[Kr] $4d^{10}$ $5s^2$ $5p^4$. For structural and electronic parameter calculations, a $2 \times 2 \times 1$ supercell of 2D 2H-$WTe_2$ unit cell was designed. For phonon dispersion investigations, a $4 \times 4 \times 1$ supercell of 2D 2H-$WTe_2$ unit cell was developed. The energy cutoff is attained at 55 Ry (750 eV) with a tolerance of less than 0.0005 eV and the Brillion zone with the Monkhorst–Pack arrangement for $k$-point grids $12 \times 12 \times 1$ is considered for the monolayer. The equilibrium atomic structure is optimized by relaxing lattice atomic coordinates with a tolerance of less than $0.001 \frac{eV}{Å}$ for each atom in the structure and these convergence tests are acceptable according to the standards for the next calculations. Under these conditions, the lattice parameters $a = b$ and the vacuum space, normal to the plane of the layer are calculated and 15Å is used for this work. Tensile and compressive straining circumstances are taken into consideration in two dimensions parallel to the layer plane following optimization of the equilibrium lattice parameters. The structural, electrical, lattice vibration, and optical properties are computed under both stressed and unstrained circumstances. Biaxial strain is applied to the monolayer to the desired properties from 2% tension to 2% compression ratios to analyze the electronic property, lattice vibration, and dielectric function.

The effective Hubbard parameter ($U_{eff}$) was determined iteratively for W-d orbitals using a linear response formalism utilizing DFPT with an ortho-atomic projection method [22, 23]. The Hubbard parameters are calculated independently for three cases using theQE package and are described in Table 1.

Table 1: The calculated effective Hubbard parameter for $WTe_2$ for 2% biaxial compression strain, unstrained, and 2% biaxial stress–strain.

| Structure | $U_{eff}$ (eV) W(d) orbitals |
|---|---|
| 2% Biaxial compression strain | 3.036 |
| Unstrained (equilibrium) | 3.045 |
| 2% Biaxial stress–strain | 3.053 |

## 3. Result and Discussion

*3.1. Crystal Structure.* The crystal structure of 2D 2H-$WTe_2$ is described in Figure 1. In monolayer of 2D 2H-$WTe_2$, $c$ is a constant which determines the inter layer distance and the monolayer is characterized by in plane lattice constant $a = b$. After relaxing the structure in a unit cell to minimum total energy, the lattice constant for a unit cell of 2D 2H-$WTe_2$ is found to be 3.565 Å (GGA) and 3.539 Å (GGA + U). The calculated lattice constants are compared and are in good agreement with the previous theoretical results as shown in Table 2.

We have seen the structural properties computing important parameters to check the structural stability of $WTe_2$ monolayer. The computed structural parameters for the layer are in a good agreement with the Birch Murnaghan equation of state (EOS) [24] given by

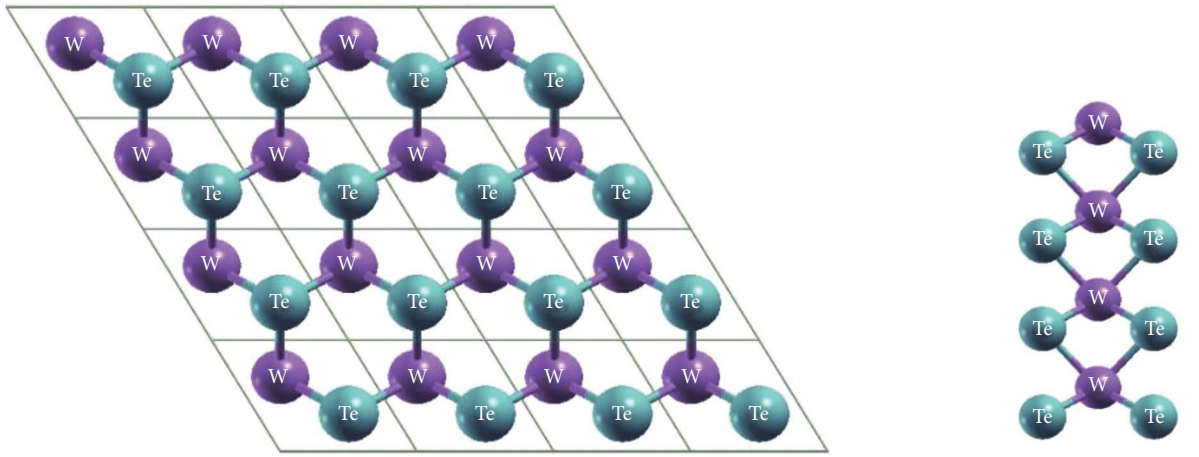


Figure 1: Structure of $WTe_2$ monolayer with the transition metal sandwiched between the chalcogen atoms.

Table 2: Calculated values for structural parameters of 2H-$WTe_2$ monolayer.

| Methods | Lattice para. (Å) | $V_0$ (Ç°³) | $B$ (Gpa) | $B'$ |
|---|---|---|---|---|
| GGA | 3.565 | 655.04 | 50.3 | 4.32 |
| GGA + U | 3.539 | 641.45 | — | — |
| Others | 3.57 [7], 3.59 [8], 3.55 [25, 26] | | | |
| Experimental | — | — | — | — |

$$E(v) = E_0 + \frac{B_0 V}{B_0' - 1}\left[\frac{\left(\frac{v_0}{v}\right)^{B_0'}}{B_0' - 1} + 1\right] - \frac{B_0 V_0}{B_0' - 1}, \quad (1)$$

where $E_0$ is for minimum energy, $V_0$ is volume of the unit cell, $B_0$ is bulk modulus and $B_0'$ is derivative of the bulk modulus.

The calculated volume versus energy and volume versus pressure diagrams are indicated for 2H-$WTe_2$ monolayer of $2 \times 2 \times 1$ supercell is described in Figure 2. Moreover, the obtained results are explained in Table 2.

*3.2. Electronic Properties: Band Structures and Density of States (DOS).* Different methods have been applied when analyzing the electronic properties of the system including the Hubbard model. The band structure of monolayer $WTe_2$ is shown in Figure 3 (a)–3(c) and it has a direct band gap. When the system is imposed to small strain (0%–2%) both in tension and compression, the band gap increases with biaxial compression and decreases with biaxial tensile strain.

The band structure of monolayer 2D 2H-$WTe_2$ using GGA and GGA + U approximations for exchange correlation potentials has been indicated in Figure 3 with the black (solid) line and magenta (broken) line, respectively. The band gap values obtained for 2% biaxial compression of the system are 1.1487 eV (GGA) and 1.2332 eV (GGA + U), respectively, as shown in Figure 3(a). For unstrained condition, the band gap values are 1.0439 eV (GGA) and 1.1089 eV (GGA + U) as described in Figure 3(b). In case of 2% biaxial tensile strain the band gap values are 0.9439 eV (GGA) and 0.9945 eV (GGA + U) as demonstrated in Figure 3(c). Moreover, the obtained band gap values are compared with the previous theoretical results and shown in Table 3. We determined some basic and important properties of the 2D 2H-$WTe_2$ from these computations. The Hubbard on site correction improves the band gap value of the monolayer as expected. Moreover, the band gap value is amplified when the compressive biaxial strain is applied to the monolayer. However, the band gap of the monolayer decreases in the presence of tensile biaxial strain. This result is in contrast to the trend observed in black SiSe monolayer in which the band gap increases with the tensile biaxial strain and reduces in the presence of compressive biaxial strain as investigated in [27]. The direct band gap cannot be altered by small strain and this may result in materials preferable for some electronic and optical properties. Moreover, the effect of electron–electron interaction in the band diagram is noticeable with the same manner in both strained and unstrained conditions and hence the Hubbard correction is significant for the system. The range of band gap values of monolayer 2D 2H-$WTe_2$ both in unstrained and strained conditions are interesting for the photovoltaic applications.

In addition to the band structure, the total density of states (TDOS) was calculated for 2% biaxial compression, unstrained, and 2% biaxial tensile strain using GGA and GGA + U approximation for exchange correlation potentials as shown in Figure 4(a)–4(c), respectively. The gap from the valence band maximum to the conduction band minimum decreases when the system is imposed to biaxial tensile strain than the biaxial compression. Moreover, the partial density of states (PDOS) was also calculated using GGA and GGA + U approximation for exchange correlation potential and described in Figures 5(a) and 5(b). The PDOS result

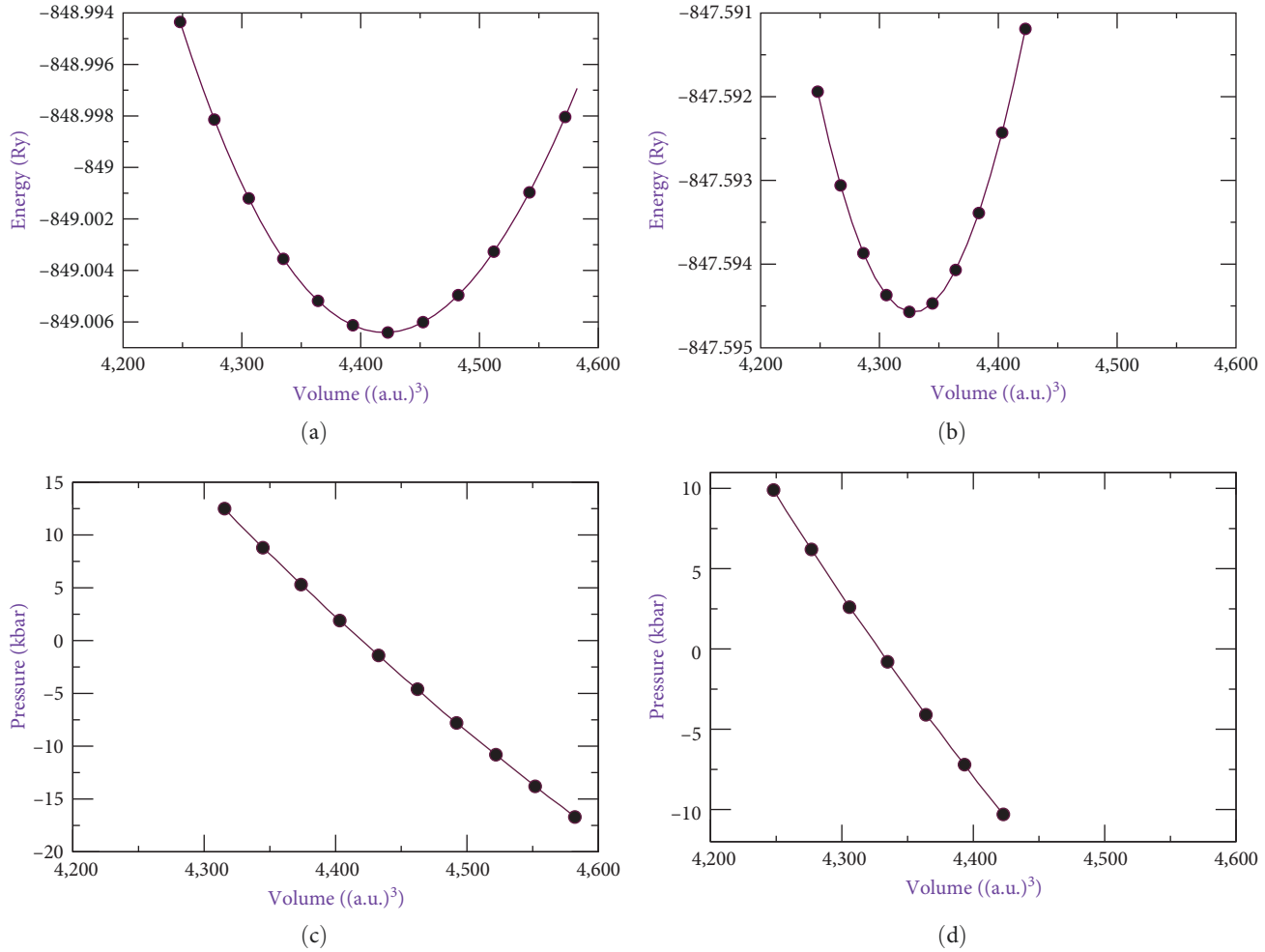


FIGURE 2: Volume versus energy diagram of 2H-$WTe_2$ using (a) GGA (b), GGA + U and pressure versus volume diagram using, (c) GGA, and (d) GGA + U.

describes that for the low-lying states, the W (3d) orbitals contributed most to the maximum valence band and minimum conduction band.

*3.3. Phonon Vibration.* Concerning the lattice vibration, it is important to know the dynamic property of the material for its stability. We have calculated the phonons dispersion for 2% biaxial compression, unstrained, and 2% biaxial tensile strain in accord with DFPT and DFPT + U for exchange-correlation potential, respectively, as shown in Figure 6(a)–6(c). The obtained result for DFPT shows that the unstrained condition is dynamically stable and has no imaginary part as shown in Figure 6(b). However, when the monolayer of 2H-$WTe_2$ is subjected to biaxial strain the dispersion relation has negative frequency and it is dynamically unstable with respect to DFPT as described in Figures 6(a) and 6(c), respectively. However, the phonon dispersions obtained for biaxial compression, unstrained, and biaxial tensile strain using the Hubbard correction (DFPT + U) are dynamically stable as described in Figure 6 (magenta, broken lines). That is, DFPT + U is used to capture the effect of electronic localization of vibrational frequencies and give full access to the all quantities requiring well-converged sums over the entire vibration spectrum.

*3.4. Optical Properties.* To calculate the optical properties, the complex dielectric function $\varepsilon(\omega)$ within an independent particle formalism is used [28];

$$\varepsilon = \varepsilon_1(\omega) + i\varepsilon_2(\omega). \tag{2}$$

The imaginary part $\varepsilon_2(\omega)$ is determined from the momentum dipole transition matrix elements between the valence band and the conduction band electronic states with long wavelength approximations [29],

$$\varepsilon_2^{ij}(\omega) = \frac{4\pi^2 e^2}{Vm\omega^2} \times \sum_{knn'\sigma} \langle \chi_{n\sigma}|u_\alpha|\chi_{n'\sigma}\rangle\langle \chi_{n'\sigma}|u_\beta|\chi_{n\sigma}\rangle \times f_{kn}(1 - f_{kn'})\sigma(\epsilon_{kn'} - \epsilon_{kn} - \hbar\omega), \tag{3}$$

where $\langle \chi_{n\sigma}|$ and $|\chi_{n'\sigma}\rangle$ are the electron states. The dispersion of the real part of the dielectric function $\varepsilon_1(\omega)$ was determined using the imaginary part by Kramers–Kronig relations [30],

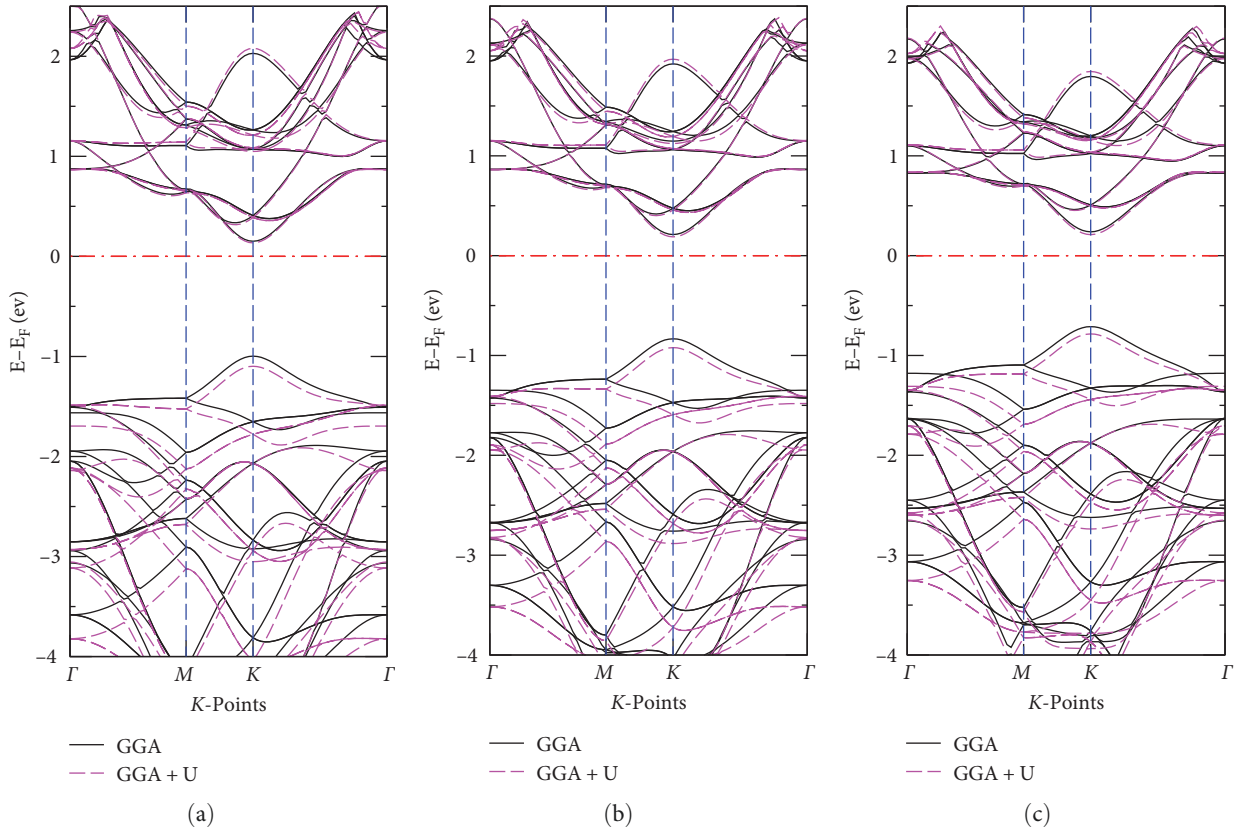


FIGURE 3: Band structure of 2H-$WTe_2$ (a) 2% biaxial compression, (b) unstrained, and (c) 2% biaxial tensile strain using GGA and GGA + U.

TABLE 3: The band gap values of monolayer 2H-$WTe_2$ with respect to GGA and GGA + U.

| | GGA | GGA + U | Others | Exp't. |
|---|---|---|---|---|
| Band gap (eV) unstrained | 1.0439 | 1.1089 | 0.974 (GGA) [8] 0.75 (GGA) [26] | — |
| Band gap (eV) 2% biaxial compression | 1.1487 | 1.2332 | — | — |
| Band gap (eV) 2% biaxial tensile strain | 0.9439 | 0.9945 | — | — |

$$\varepsilon_1(\omega) = 1 + \frac{2}{\pi} \mathrm{P} \int_0^{\infty} \frac{\omega' \varepsilon_2(\omega')}{\omega'^2 - \omega^2} d\omega'. \tag{4}$$

The symbol $P$ represents the principal value of the integral. The complex index of refraction is written as follows:

$$\tilde{n}(\omega) = n(\omega) + ik(\omega). \tag{5}$$

Here, $n(\omega)$ is refractive index and $k(\omega)$ is extinction coefficient that can be evaluated from complex dielectric function. The refractive index ($n(\omega)$), the reflectivity ($R(\omega)$), absorption coefficient ($\alpha(\omega)$), and energy loss function ($L(\omega)$) can be determined from the dielectric functions by,

$$\begin{aligned} n(\omega) &= \left( \frac{\varepsilon_1(\omega) + \sqrt{\varepsilon_1(\omega)^2 + \varepsilon_2(\omega)^2}}{2} \right)^{\frac{1}{2}}, \qquad \alpha(\omega) = 2\sqrt{\omega} \left( \sqrt{\varepsilon_1(\omega)^2 + \varepsilon_2(\omega)^2} - \varepsilon_1(\omega) \right)^{1/2}, \\ R(\omega) &= \frac{(n(\omega) - 1)^2 + k(\omega)^2}{(n(\omega) + 1)^2 + k(\omega)^2}, \qquad L(\omega) = -Im \frac{1}{\varepsilon(\omega)} = \frac{\varepsilon_2(\omega)}{\varepsilon_1(\omega)^2 + \varepsilon_2(\omega)^2}. \end{aligned} \tag{6}$$

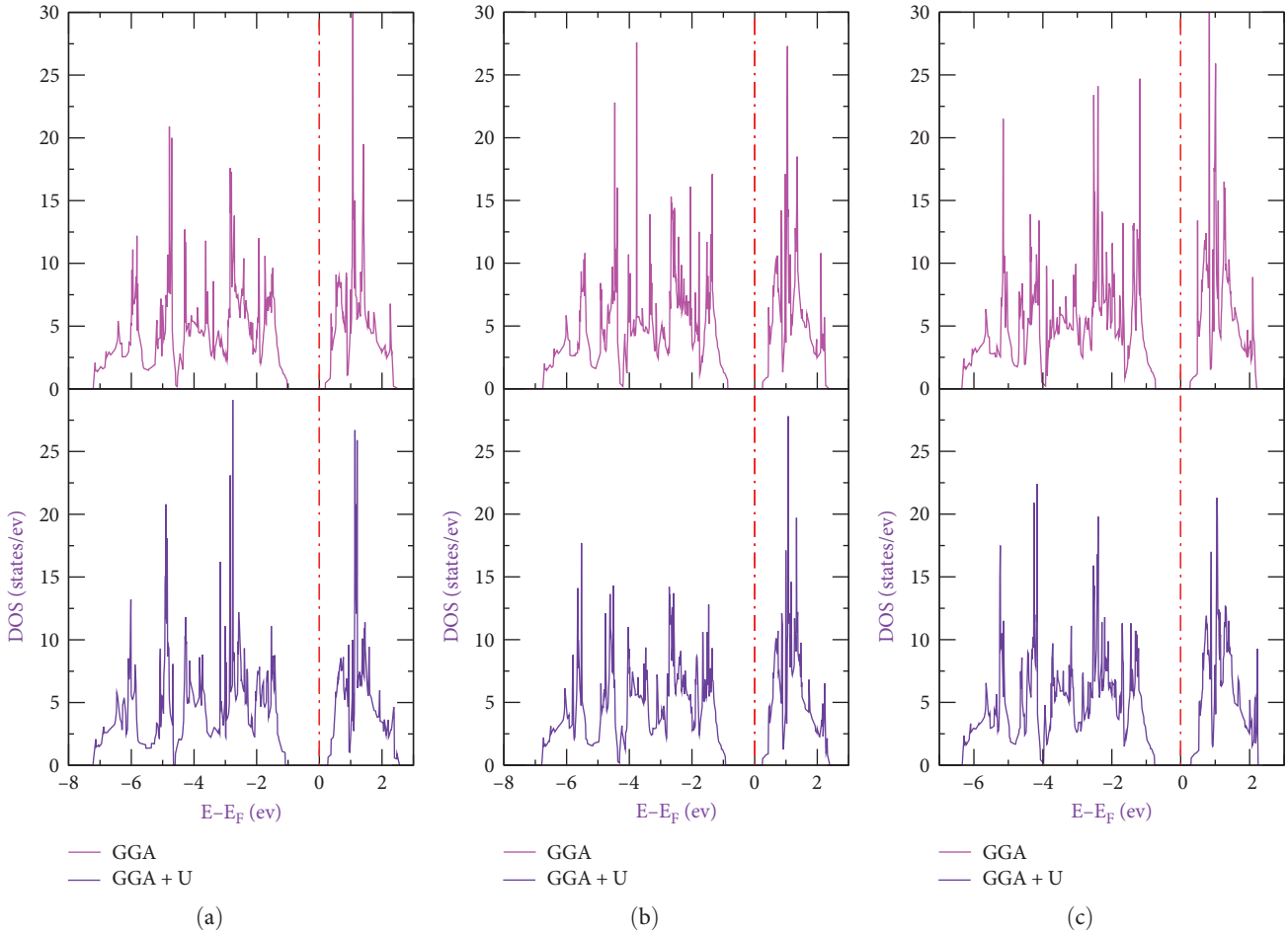


FIGURE 4: The density of states (a) with −2% biaxial strain, (b) with no strain, and (c) with + 2% biaxial strain.

The optical properties including dielectric function, optical absorption, and energy loss function, reflectivity, and the refractive index are investigated in parallel and perpendicular direction to the plane of the monolayer 2H-$WTe_2$ in the photon energy range from 0 to 10 eV, and the details of the calculations are presented.

The real part of the dielectric function ($\varepsilon_1(\omega)$) when the monolayer of 2H-$WTe_2$ is exposed to the polarization parallel and perpendicular direction to the monolayer plane is shown in Figures 7(a) and 7(b), respectively. From the figure it is possible to deduce that the static dielectric function values for $\varepsilon_1(0)$ is 10.6 (unstrained), 7.6 (biaxial strain), and 7.3 (biaxial compression) arbitrary unit for the polarization parallel to the plane of monolayer. However, the static dielectric constant $\varepsilon_1(0)$ decreases when the polarization is perpendicular to the plane of monolayer and the values are 4.38 (unstrained) and 1.9 for biaxial compression or strain. The magnitude of the real part of the dielectric function for the polarization parallel to the plane is magnified as compared to the perpendicular direction. The peak of the real part of the dielectric constant is 14.9 at 0.9 eV for biaxial tensile strain, 17.7 at 1 eV for unstrained, and 14.9 at 1.1 eV for biaxial compression (parallel to the plane) and 4.2 at 4.1 eV for biaxial tensile strain, 12.5 at 4.5 eV for unstrained, and 4.2 at 4.8 eV for biaxial compression (perpendicular to the plane). Moreover, the peak of linear dielectric function for the polarization perpendicular to the plane of monolayer shifts toward high energy for all cases. The biaxial compression and tensile stress also reduce the magnitude of the real part of the dielectric function as compared to the unstrained one. On the other hand, the imaginary part of the dielectric function is described in Figure 7(c) for the polarization parallel to the plane and Figure 7(d) perpendicular to the plane with respect to the incoming photon. The imaginary part of the dielectric function has a peak value 16.25 at 0.9 eV for biaxial tensile strain, 18.5 at 3.9 eV for unstrained, and 16.3 at 1.1 eV for biaxial compression, respectively, when the polarization is parallel to the plane of monolayer. The peak value is 7.5 at 4.1 eV for biaxial tensile strain, 17.5 at 4.5 eV for unstrained, and 7.1 at 4.8 eV for biaxial compression when the polarization is perpendicular to the plane of monolayer. The magnitude of the imaginary part of the dielectric function is quenched as the monolayer of 2H-$WTe_2$ forced to tensile stress or compression. The negative value in the $\varepsilon_1(\omega)$ spectra at 4.5, 4.8, and 5 eV corresponds to the peak in the reflectivity spectra.

The other important parameters of optical properties are the refractive index $n(\omega)$ and extinction coefficient $\kappa(\omega)$ as

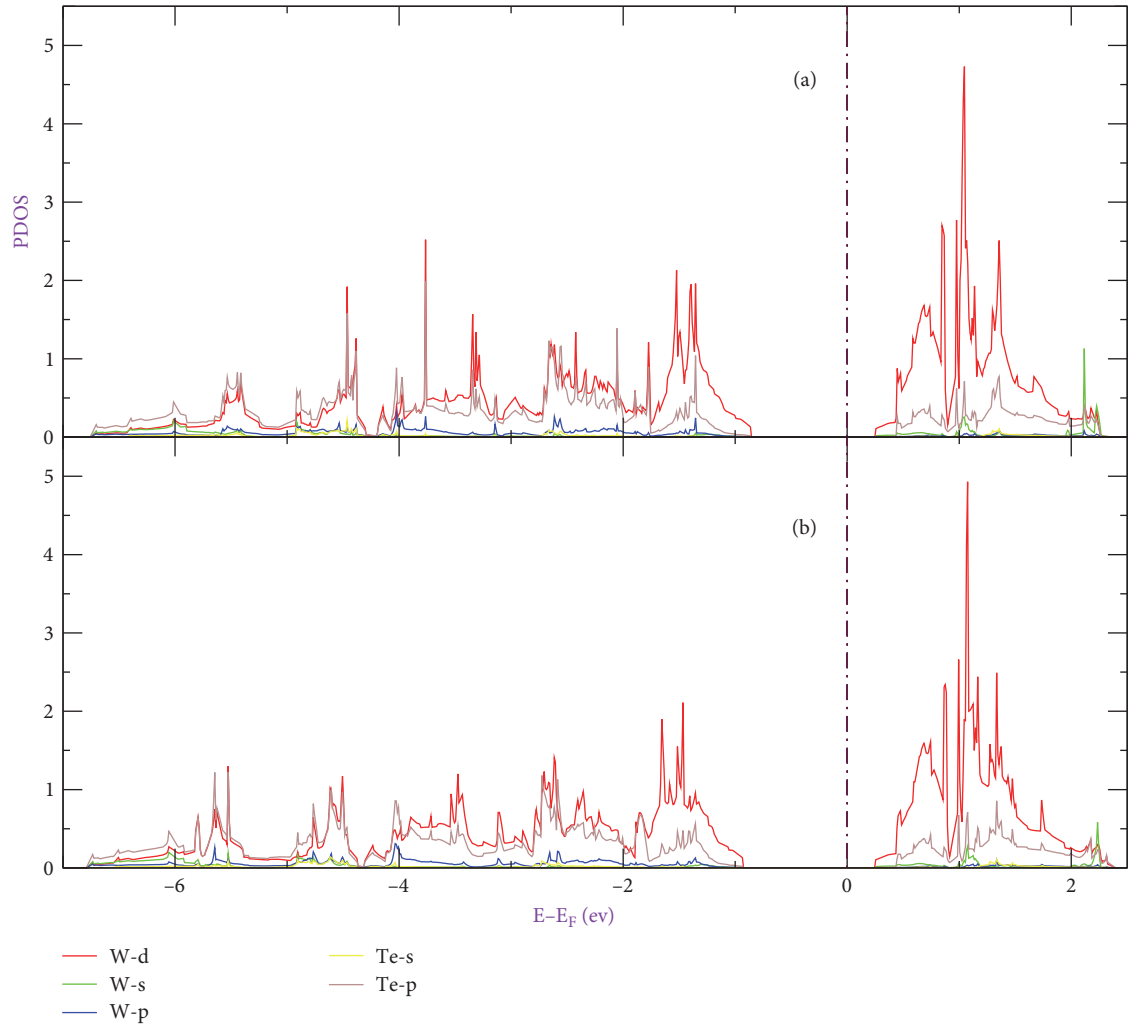


FIGURE 5: Partial density of states for unstrained monolayer of $WTe_2$ (a) using GGA and (b) GGA + U approximation.

shown in Figures 8(a) and 8(b) for polarization perpendicular to the plane of monolayer, respectively. The value of static refractive index $n(0)$ is 2.2 (unstrained) and 1.35 for biaxial compression or strain. The peak values of the refractive index are 2.5 at 4.25 eV for tensile strain, 3.85 at 4.48 eV for unstrained, and 2.5 at 4.6 eV for biaxial compression. The magnitude of the refractive index decreases when the monolayer of 2H-$WTe_2$ is imposed to tensile stress or compression. Moreover, the peak of the refractive index shifts toward higher energy when the monolayer of 2H-$WTe_2$ is imposed to biaxial compression than tensile strain. The peak value of the extinction coefficient is 1.9 at 4.3 eV for tensile stress, 2.75 at 4.5 eV for unstrained, and 2.2 at 5 eV for biaxial compression. The peak value of the extinction coefficient for monolayer of $WTe_2$ shows blue shift as compared to the tensile stress.

The absorption coefficient of monolayer 2H-$WTe_2$ for unstrained, biaxial compression, and biaxial tensile strain is also described in Figure 9(a)–9(c), respectively. The peaks of the absorption coefficients are $1.5 \times 10^6 cm^{-1}$ at 8.0636 eV (2% biaxial compression), $1.51 \times 10^6 cm^{-1}$ at 7.54 eV (unstrained), and $1.45 \times 10^6 cm^{-1}$ at 7.15 eV (2% biaxial tension). The magnitude of the absorption coefficient of the monolayer of 2H-$WTe_2$ has a little variation in three cases. However, red shift is observed when the monolayer is imposed to biaxial tension as compared to the biaxial compression. This result is a consequence of the variation of the band gap value from 1.2332 to 0.9945 eV as the monolayer is exposed to a biaxial compression and biaxial tensile stress. The large value of absorption coefficient in 2H-$WTe_2$ monolayer coupled with its optimum band gap enables it for application of solar cell with high-power conversion efficiency.

The electron energy loss function of monolayer 2H-$WTe_2$ for unstrained, biaxial compression, and biaxial tensile strain is described in Figure 9(d)–9(f), respectively. The energy loss function (EELS) which shows the energy loss of fast electron moving across the medium is a complicated mixture of interband transition and plasmon. The electron energy loss spectra are related to the plasma frequency. Peaks in the measured spectra can thus derive zeros of $\varepsilon_1(\omega)$ (when

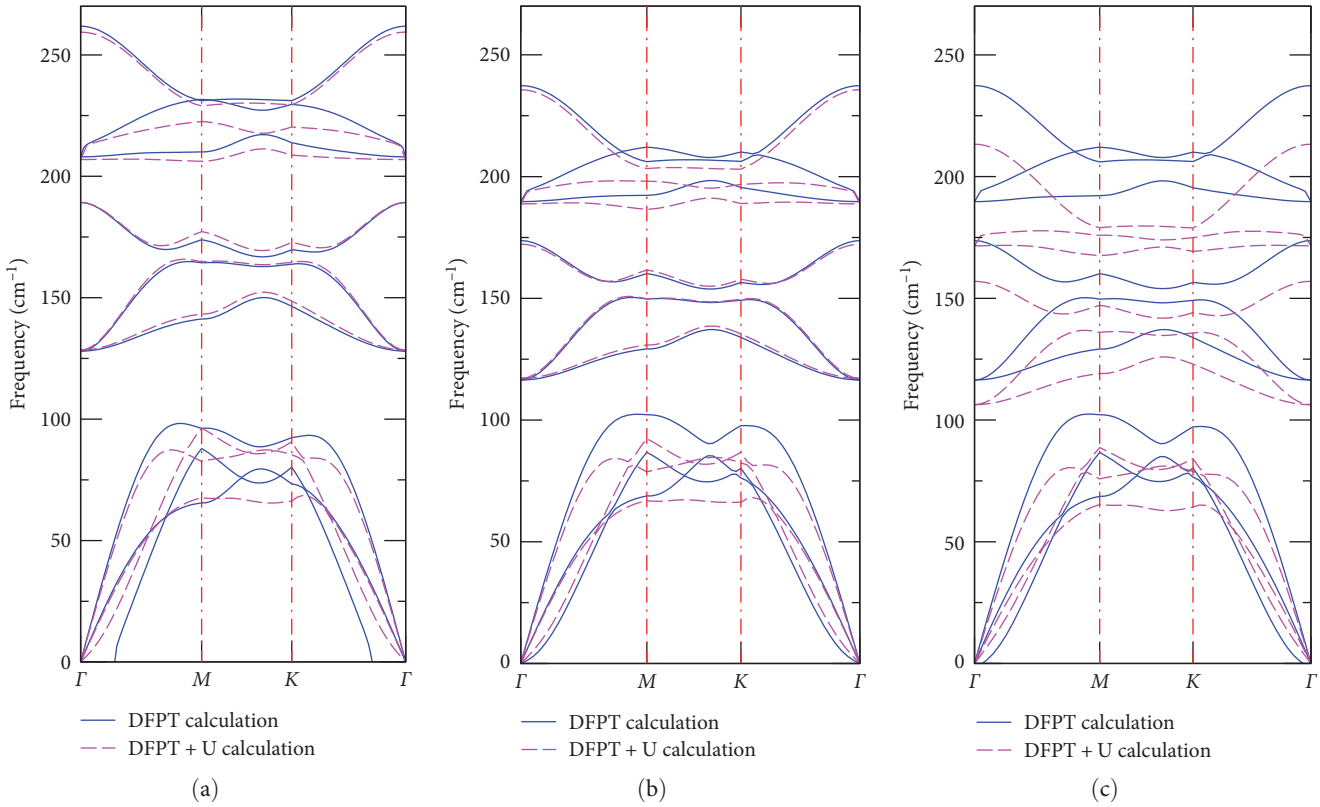


Figure 6: Phonon dispersion for (a) the compressed (−2% strain), (b) undisturbed (unstrained), and (c) stretched monolayer (+2% strained) of 2H-$WTe_2$.

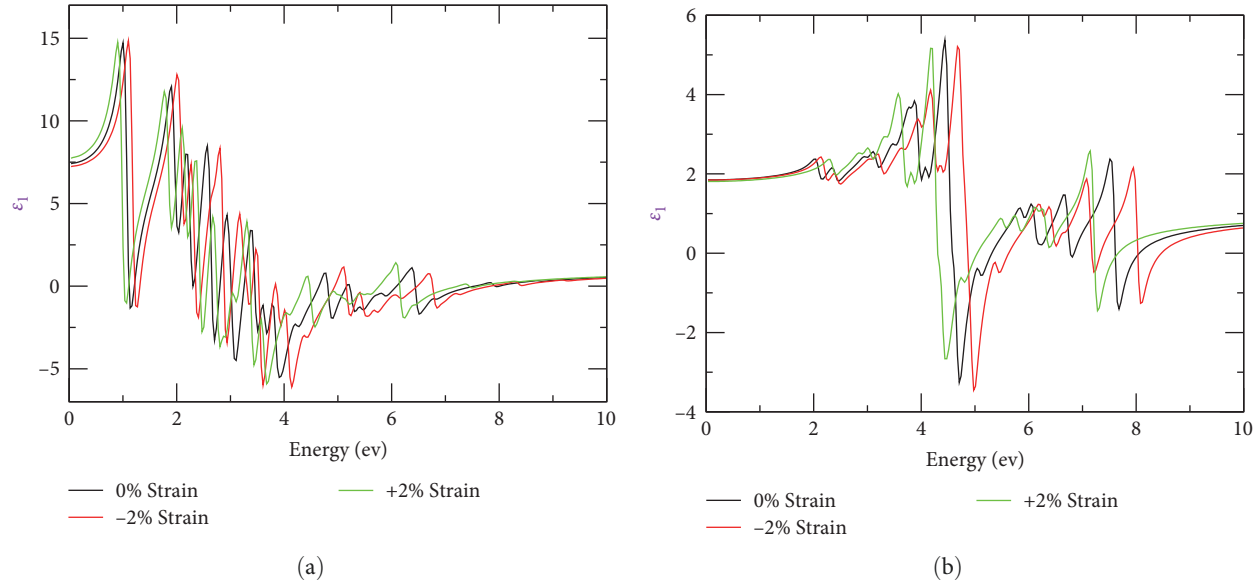


Figure 7: Continued.

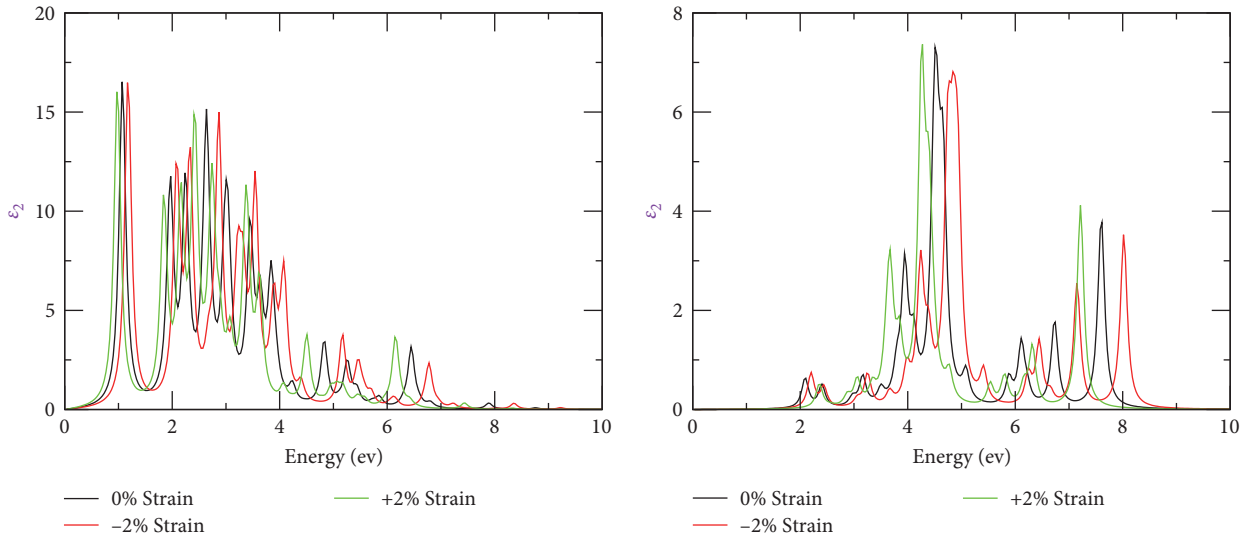


FIGURE 7: The real and imaginary part of the dielectric function versus photon energy (a and c) with polarization parallel to the plane and (b and d) perpendicular to the plane, respectively, for the monolayer of 2H-$WTe_2$.

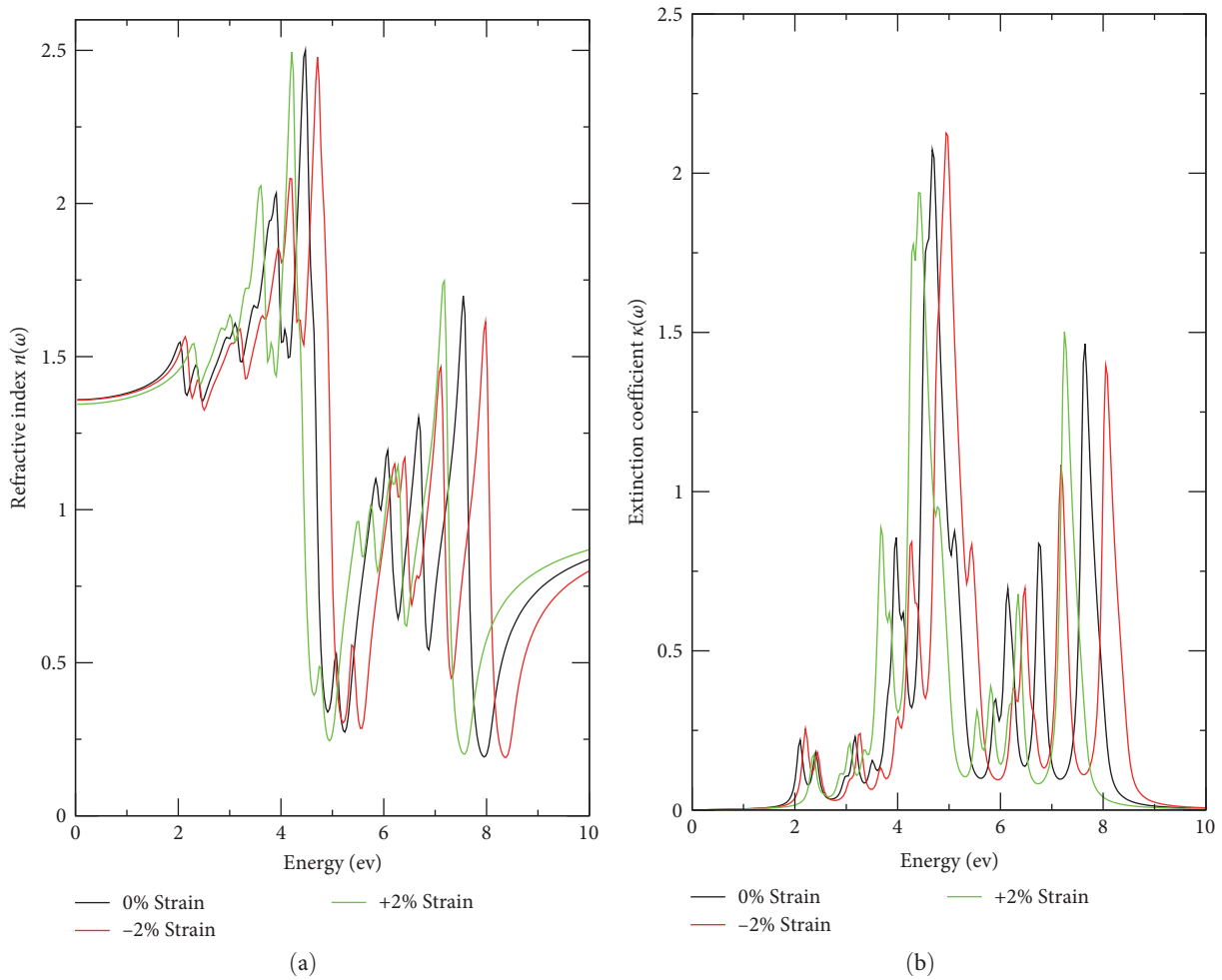


FIGURE 8: (a) Refractive index and (b) extinction coefficient with different strain conditions to the plane of the $WTe_2$ layer.

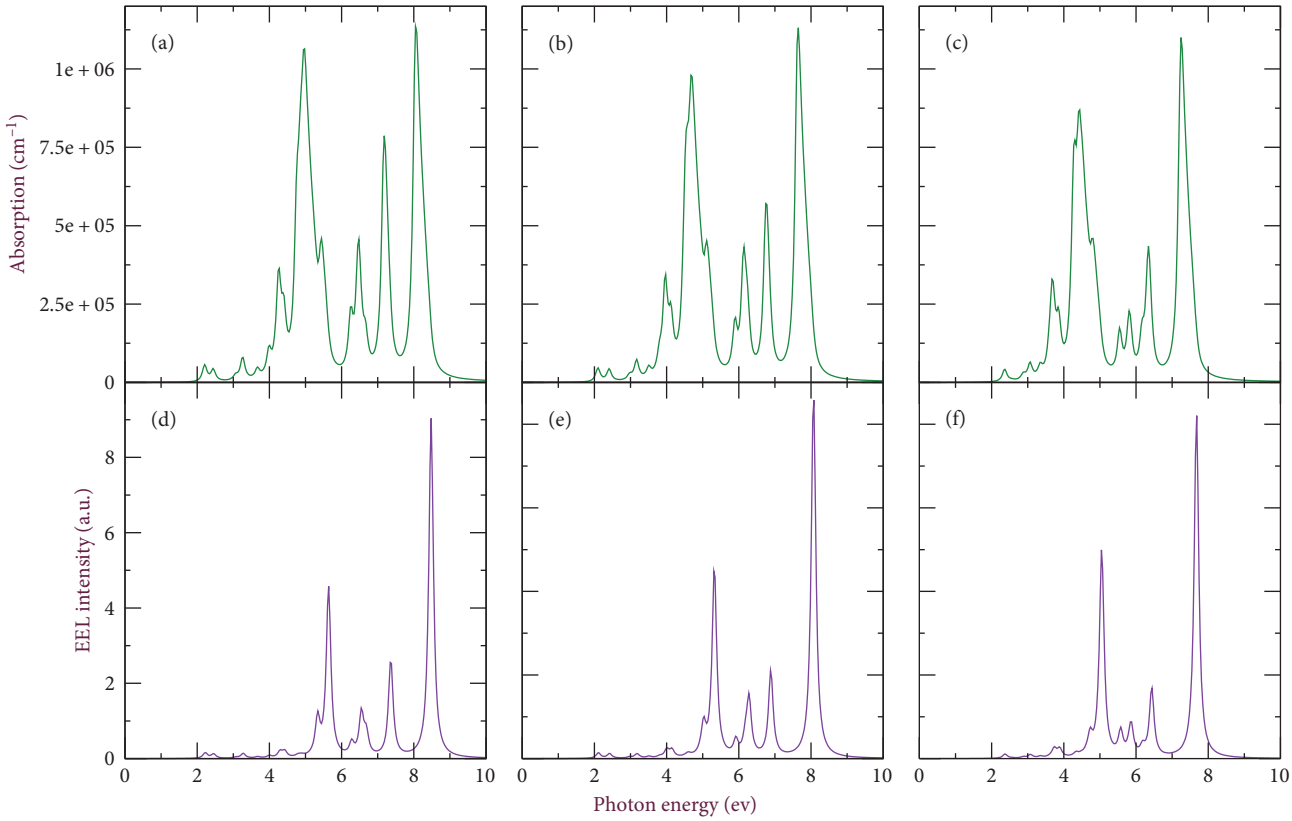


FIGURE 9: Absorption coefficient and electron energy loss function of the monolayer 2H-$WTe_2$ with (a and d) no strain, (b and e) −2% strain, and (c and f) + 2% strain, respectively.

$\varepsilon_2$ ($\omega$) is not too large), which correspond to the collective plasmon excitations, or from structures $\varepsilon_2$ ($\omega$) which are due to valence-conduction interband transitions. The electron energy loss function for a polarization perpendicular to the plane of monolayer has a peak 9.1 at 8.5 eV (unstrained), 9.6 at 8.1 eV (biaxial compression), and 9.2 at 7.5 eV (biaxial strain).

Finally, the reflectivity is computed for unstrained (a), biaxial compression (b), and biaxial stress (c) as shown in Figure 10 for polarization perpendicular to the plane of monolayer 2H-$WTe_2$. The value of static reflectivity $R(0)$ are 12.5%, 4.2%, and 12.5% for biaxial compression, unstrained, and biaxial, respectively. The peak values of optical reflectivity are 52% at 4.8 eV (biaxial compression), 65% at 5 eV (unstrained), and 52% at 4.9 eV (biaxial stress).

## 4. Conclusions

In this study we have used the first principle calculations implemented in QE software package to study the structural, electronic, dynamic, and optical properties of 2D 2H-$WTe_2$ monolayer. The lattice constant, bulk modulus, and the derivative of bulk modulus are calculated using GGA and GGA + U approximations for exchange correlation potentials in PBE functional. The obtained results are in good agreement with the previous theoretical results. The band gap values calculated with respect to GGA are 1.0439, 1.1487, and 0.9439 eV for unstrained, 2% biaxial compression, and 2% biaxial tensile strain, respectively. However, the band gap values determined using GGA + U approximations for exchange correlation potential are 1.1089, 1.2332, and 0,9945 eV for unstrained, biaxial compression, and biaxial tensile strain, respectively. The onsite Hubbard corrections are used to remove self-interaction in the band gap of the monolayer 2H-$WTe_2$. Moreover, the discontinuity of TDOS from the valence band maximum to conduction band minimum reproduces the obtained band gap values. In addition to this imposing the monolayer to a small amount biaxial compression or tensile stress tunes the band gap value without altering the direct band gap nature of the system. The phonon dispersion is calculated for 2% biaxial compression, unstrained, and 2% biaxial tensile stress using DFPT and DFPT + U. The DFPT result shows that the phonon dispersion calculated for unstrained condition is stable. In contrast to this the phonon dispersion obtained employing DFPT for the biaxial compression and tensile stress are not dynamically stable. On the other hand, the phonon dispersions determined using DFPT + U are dynamically stable for unstrained and strained conditions. This is due to the consequence that DFPT + U is used to capture the effect of electronic localization of vibrational frequencies over the entire vibrational spectrum. Finally, the optical properties of 2D 2H-$WTe_2$ monolayer such as real and imaginary part of the dielectric

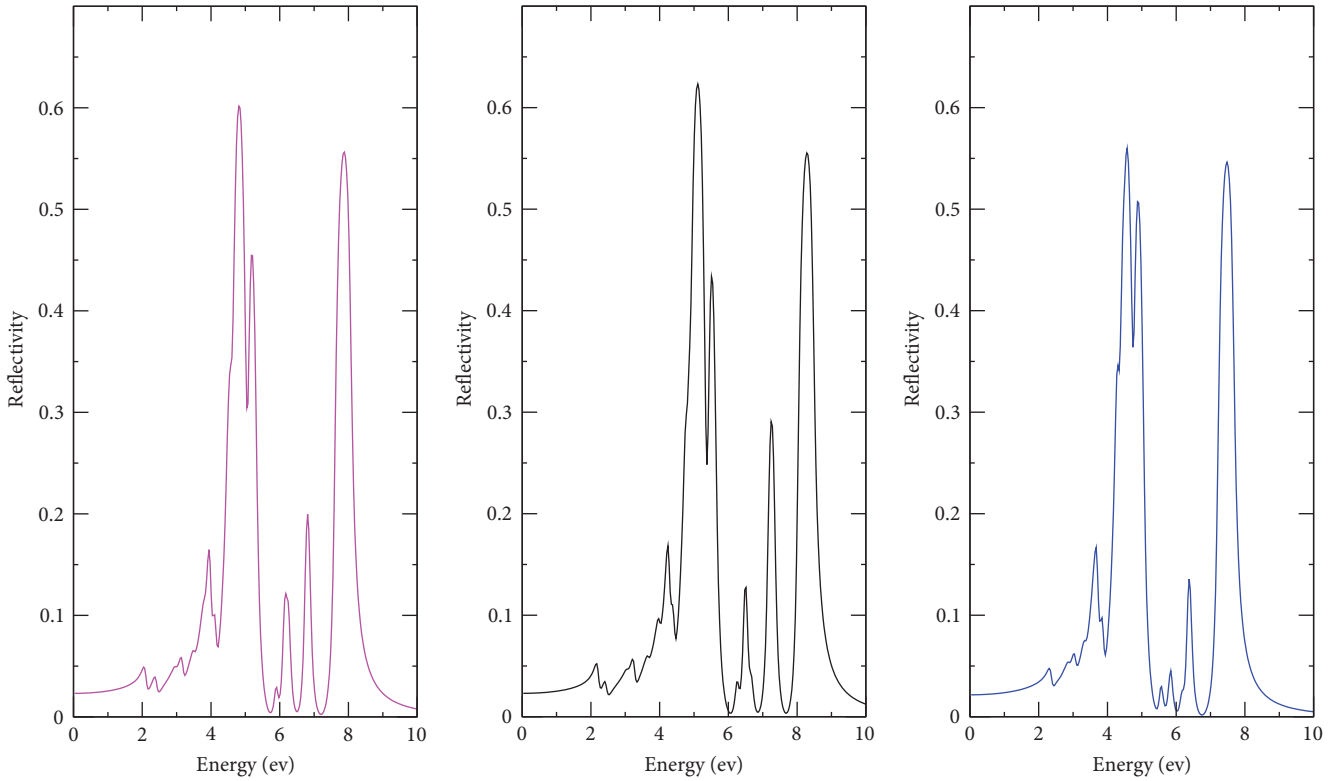


Figure 10: Reflectivity of the layer for (a) unstrained, (b) −2% strained, and (c) +2% strained.

function, refractive index, absorption coefficient, electron energy loss function, and the reflectivity are investigated. The high-absorption power in the visible spectral region complemented with the direct band gap make 2D 2H-$WTe_2$ the best candidate for photovoltaic devices. After all the experimental verification of the electronic, phonon dispersion, and optical properties of the monolayer 2H-$WTe_2$ are recommended in the future works.

## Data Availability

The data used to support the findings of this study are included within the article.

## Conflicts of Interest

The authors declare that they have no conflicts of interest.

## Acknowledgments

The authors express their thanks and appreciation to the Department of Physics, College of Natural Sciences, Jimma University (grant number: CNSPHYS-04-2021/2022), for financially supporting the Ph.D. student.

## References

[1] A. Ramasubramaniam, D. Naveh, and E. Towe, "Tunable band gaps in bilayer transition-metal dichalcogenides," *Physical Review B*, vol. 84, no. 20, 2011.

[2] X. Zhang, Y. Sun, W. Gao et al., "Sizable bandgaps of graphene in 3d transition metal intercalated defective graphene/$WSe_2$ heterostructures," *RSC Advances*, vol. 9, no. 32, pp. 18157–18164, 2019.

[3] J. Gusakova, X. Wang, L. L. Shiau et al., "Electronic properties of bulk and monolayer TMDs: theoretical study within DFT framework (GVJ-2e method)," *Physica Status Solidi*, vol. 214, no. 12, 2017.

[4] B. R. Sutherland, "Solar materials find their band gap," *Joule*, vol. 4, no. 5, pp. 984-985, 2020.

[5] L. Loh, Z. Zhang, M. Bosman, and G. Eda, "Substitutional doping in 2D transition metal dichalcogenides," *Nano Research*, vol. 14, no. 6, pp. 1668–1681, 2021.

[6] M. Fang and E.-H. Yang, "Advances in two-dimensional magnetic semiconductors via substitutional doping of transition metal dichalcogenides," *Materials*, vol. 16, no. 10, Article ID 3701, 2023.

[7] B. Amin, T. P. Kaloni, and U. Schwingenschlögl, "Strain engineering of $WS_2$, $WSe_2$, and $WTe_2$," *RSC Advances*, vol. 4, no. 65, Article ID 34561, 2014.

[8] M. R. Islam, M. R. H. Mojumder, B. K. Moghal et al., "Impact of strain on the electronic, phonon, and optical properties of monolayer transition metal dichalcogenides $XTe_2$ (X = Mo and W)," *Physica Scripta*, vol. 97, no. 4, Article ID 045806, 2022.

[9] S. Deng, A. V. Sumant, and V. Berry, "Strain engineering in two-dimensional nanomaterials beyond graphene," *Nano Today*, vol. 22, pp. 14–35, 2018.

[10] H. Guo, N. Lu, L. Wang, X. Wu, and X. C. Zeng, "Tuning electronic and magnetic properties of early transition-metal dichalcogenides via tensile strain," *The Journal of Physical Chemistry C*, vol. 118, no. 13, pp. 7242–7249, 2014.

[11] S. Roy and P. Bermel, "Electronic and optical properties of ultra-thin 2D tungsten disulfide for photovoltaic applications," *Solar Energy Materials and Solar Cells*, vol. 174, pp. 370–379, 2018.

[12] Y. Li, A. Chernikov, X. Zhang et al., "Measurement of the optical dielectric function of monolayer transition-metal dichalcogenides: $MoS_2$, $MoSe_2$, $WS_2$, and $WSe_2$," *Physical Review B*, vol. 90, no. 20, 2014.

[13] B. K. Moghal and M. R. Islam, "Tuning the electronic, phonon, and optical properties by strain-induced on the monolayer transition metal dichalcogenides ASe2 (A = Mo and W)," *Materials Today Communications*, vol. 31, Article ID 103240, 2022.

[14] V. I. Anisimov, Ferdi Aryasetiawan, and A. I. Lichtenstein, "First-principle calculations of the electronic structure and spectra of strongly correlated systems: the LDA+ U method," *Journal of Physics: Condensed Matter*, vol. 9, no. 4, Article ID 767, 1997.

[15] S. L. Dudarev, G. A. Botton, S. Y. Savrasov, C. J. Humphreys, and A. P. Sutton, "Electron-energy-loss spectra and the structural stability of nickel oxide: an LSDA + U study," *Physical Review B*, vol. 57, no. 3, pp. 1505–1509, 1998.

[16] P. Giannozzi, S. de Gironcoli, P. Pavone, and S. Baroni, "*Ab initio* calculation of phonon dispersions in semiconductors," *Physical Review B*, vol. 43, no. 9, pp. 7231–7242, 1991.

[17] A. Floris, S. de Gironcoli, E. K. U. Gross, and M. Cococcioni, "Vibrational properties of MnO and NiO from DFT+U-based density functional perturbation theory," *Physical Review B*, vol. 84, no. 16, 2011.

[18] J. P. Perdew, K. Burke, and M. Ernzerhof, "Generalized gradient approximation made simple," *Physical Review Letters*, vol. 77, no. 18, pp. 3865–3868, 1996.

[19] P. Giannozzi, O. Andreussi, T. Brumme et al., "Advanced capabilities for materials modelling with quantum ESPRESSO," *Journal of Physics: Condensed Matter*, vol. 29, no. 46, Article ID 465901, 2017.

[20] P. Giannozzi, S. Baroni, N. Bonini et al., "QUANTUM ESPRESSO: a modular and open-source software project for quantum simulations of materials," *Journal of Physics: Condensed Matter*, vol. 21, no. 39, Article ID 395502, 2009.

[21] D. Vanderbilt, "Soft self-consistent pseudopotentials in a generalized eigenvalue formalism," *Physical Review B*, vol. 41, no. 11, pp. 7892–7895, 1990.

[22] A. Floris, I. Timrov, B. Himmetoglu, N. Marzari, S. de Gironcoli, and M. Cococcioni, "Hubbard-corrected density functional perturbation theory with ultrasoft pseudopotentials," *Physical Review B*, vol. 101, no. 6, 2020.

[23] I. Timrov, N. Marzari, and M. Cococcioni, "Self-consistent Hubbard parameters from density-functional perturbation theory in the ultrasoft and projector-augmented wave formulations," *Physical Review B*, vol. 103, no. 4, Article ID 045141, 2021.

[24] F. Birch, "Finite elastic strain of cubic crystals," *Physical Review*, vol. 71, no. 11, pp. 809–824, 1947.

[25] E. Torun, H. Sahin, S. Cahangirov, A. Rubio, and F. M. Peeters, "Anisotropic electronic, mechanical, and optical properties of monolayer WTe2," *Journal of Applied Physics*, vol. 119, no. 7, 2016.

[26] M. Zulfiqar, Y. Zhao, G. Li, Z. C. Li, and J. Ni, "Intrinsic thermal conductivities of monolayer transition metal dichalcogenides MX2 (M = Mo, W; X = S, Se, Te)," *Scientific Reports*, vol. 9, no. 1, 2019.

[27] S. Behzad and R. Chegel, "Engineering the light absorption spectrum and electronic properties of black and blue phases of a SiSe monolayer via biaxial straining," *Journal of Computational Electronics*, vol. 22, no. 4, pp. 971–981, 2023.

[28] J. E. Sipe and E. Ghahraman, "Nonlinear optical response of semiconductors in the independent-particle approximation," *Physical Review B*, vol. 48, no. 16, pp. 11705–11722, 1993.

[29] P. Ondračka, D. Holec, and L. Zajíčková, "Predicting optical properties from Ab-initio calculations," in *Optical Characterization of Thin Solid Films*, vol. 64 of *Springer Series in Surface Sciences*, pp. 83–104, Springer, 2018.

[30] V. B. Bobrov, S. A. Trigger, G. J. F. van Heijst, and P. P. J. M. Schram, "Kramers–Kronig relations for the dielectric function and the static conductivity of Coulomb systems," *EPL*, vol. 90, no. 1, Article ID 10003, 2010.